



Analytic Continuation of the Two-Reggeon
Cut Discontinuity Formula

A. R. WHITE
National Accelerator Laboratory, Batavia, Illinois 60510

ABSTRACT

We give a detailed treatment of the analytic continuation of the two Reggeon cut discontinuity formula from above the four-particle threshold in the t -channel down to negative t . We confirm the negative sign of the two-Pomeranchukon cut contribution to the total cross section. We show how the Mandelstam graphs can be used as a check on this result. We trace the negative sign to signature factors and use this to argue that multi-Pomeranchukon cuts should contribute to the total cross section with alternating signs.



I. INTRODUCTION

In this paper we give a detailed treatment of the analytic continuation of the discontinuity formula¹⁻³ for the two-Reggeon cut from $t > 16 \text{ m}^2$, where it is initially derived, to the scattering region $t < 0$. This continuation is not treated in sufficient detail in Ref. 2, and it has been suggested⁴ that a more detailed treatment could lead to a reversal of the claimed negative sign for the contribution of the two Pomeron cut to the total cross section. However, the analysis we present in this paper confirms that the sign is indeed negative. We emphasize that this result is based only on the combination of t-channel unitarity with standard analyticity assumptions for both multiparticle and Pomeron scattering amplitudes.

As we discuss in Sec. VII, any treatment of the two Reggeon cut based on the analytic continuation of multiparticle t-channel unitarity to complex angular momentum, must be applicable to the familiar Mandelstam Feynman graphs. It then follows from the real analyticity property of Pomeron scattering amplitudes that the sign of the two Pomeron cut in the full amplitude must be the same as that of the two-Reggeon cut given by the Mandelstam graphs, since the signature and other kinematic factors are the same in the two cases. This argument in one sense confirms our result that the sign of the two Pomeron cut is negative. Alternatively we could say that the argument actually requires us to prove that we obtain the negative sign in order to check

that the precise form of our complex angular momentum analytic continuation of multiparticle unitarity⁵ is correct. In fact we show that the negative sign for the two Pomeron cut arises directly from the signature factors in the continuation. This is in accord with the dependence on signature, of both the Mandelstam graphs and Gribov's Reggeon calculus, for producing a negative sign two Reggeon cut. We also argue that a similar treatment of signature for the multi-Pomeron cuts will lead to the (expected) general result that they contribute with alternating signs to the total cross section.

In Sec. II we give the Sommerfeld-Watson formula for the two-Reggeon cut contribution to the total cross section in order to establish notation. In Sec. III we review the derivation of the discontinuity formula and isolate where sign changes occur. In Sec. IV we discuss analytic continuation of the formula to t small but still greater than zero. This stage of the continuation can be checked directly using the Mandelstam graphs. In Sec. V we discuss the movement of mass dependent singularities off of the physical sheet of the two-Reggeon cut. In Sec. VI we discuss continuation from positive to negative t and confirm that the contribution of the two Pomeron cut to the total cross section is negative. In Sec. VII we discuss the Mandelstam graphs. Section VIII contains a short discussion of the relevance of signature for multi-Pomeron cuts.

II. THE SOMMERFELD-WATSON REPRESENTATION

The Sommerfeld-Watson transform gives the contribution of a positive signature Regge cut to the asymptotic behavior of the full amplitude as

$$A(s, t) \underset{s \rightarrow \infty}{\sim} -\frac{1}{i} \int_{j=j_c(t)}^{j=j_c(t)} dj \frac{\text{disc } a^+(j, t) 2^j \Gamma(-j) [s^j + (-s)^j]}{\cos \pi j \Gamma(-j + 1/2)}. \quad (2.1)$$

For the two Pomeron cut $j_c(0) \sim 1$. For $j \sim 1$

$$\frac{\Gamma(-j)(1 + e^{-i\pi j})}{\Gamma(-j + 1/2)\cos \pi j} \sim +\frac{i\sqrt{\pi}}{2} \quad (2.2)$$

and so

$$A(s, 0) \sim -\sqrt{\pi} \int_{j=j_c(0)}^{j=j_c(0)} dj \text{disc } a^+(j, 0) |s|^j \quad (2.3)$$

It follows then that the sign of the contribution of the two Pomeron cut to the total cross section is given by

$$-\text{sign} \left[\frac{1}{i} \text{disc } a^+(j, t) \right] \quad (2.4)$$

where

$$\text{disc } a^+(j, t) = a^+(j+i\epsilon, t) - a^+(j-i\epsilon, t) \quad (2.5)$$

where the $\pm i\epsilon$ prescriptions are with respect to the two-Pomeron cut itself.

III. THE DISCONTINUITY FORMULA

The derivation of the discontinuity formula in Ref. 2 (II) begins with the continuation to complex angular momentum of the four-particle

unitarity relation in the t-channel. The conventional S-matrix formula for the discontinuity across the four-particle cut is shown in Fig. 1. The partial-wave projection of this relation written in terms of the partial-wave amplitudes corresponding to Fig. 2 is (we use the same notation as in II)

$$a_j(t) - a_j^4(t) = \int d\rho \sum_{|n_1+n_2| \leq j} \sum_{\ell_1 \geq |n_1|} \sum_{\ell_2 \geq |n_2|} \Lambda(j, \vec{\ell}, \vec{n}) \times a_{j, \vec{\ell}, \vec{n}}^{\rightarrow}(t, t_1, t_2) a_{j, \vec{\ell}, \vec{n}}^{4 \leftarrow}(t, t_1, t_2) \quad (3.1)$$

where $(\ell_1, n_1, t_1), (\ell_2, n_2, t_2)$ label the angular momentum, the helicity and the (mass)² of two-particle sub-states, as shown in Fig. 2

$$\Lambda(j, \vec{\ell}, \vec{n}) = \frac{(2\ell_1 + 1)(2\ell_2 + 1)\Gamma(\ell_1 - n_1 + 1)\Gamma(\ell_2 - n_2 + 1)\Gamma(j - n_1 - n_2 + 1)}{\Gamma(\ell_1 + n_1 + 1)\Gamma(\ell_2 + n_2 + 1)\Gamma(j + n_1 + n_2 + 1)}$$

and $d\rho$ represents a phase-space integration

$$\int d\rho = \frac{i}{(2\pi)^5 4! 2^6} \int_{4m}^{(t^{\frac{1}{2}} - 2m)^2} dt_1 \int_{4m}^{(t^{\frac{1}{2}} - t_1^{\frac{1}{2}})^2} dt_2 \frac{\lambda^{\frac{1}{2}}(t, t_1, t_2)}{t} \left[\frac{(t_1 - 4m^2)^{\frac{1}{2}}}{t_1} \right] \left[\frac{(t_2 - 4m^2)^{\frac{1}{2}}}{t_2} \right] \quad (3.2)$$

That part of the sum in (3.1) in which n_1 and n_2 have the same sign can be continued to complex j in the form

$$-\frac{1}{16} \sin \frac{\pi}{2}(j - \tau_1') \left\{ \int d\rho \sum_{\tau_4 \tau_5} \int \frac{dn_1 dn_2}{\sin \frac{\pi}{2}(n_1 - \tau_4') \sin \frac{\pi}{2}(n_2 - \tau_5')} \right\}$$

$$\times \sum_{\substack{\ell_1 \geq |n_1| \\ \ell_2 \geq |n_2|}} \left. \frac{\Lambda(j, \vec{\ell}, \vec{n}) a_{>}^{\vec{\tau}} a_{>}^{\vec{\tau}4--}}{\sin \frac{\pi}{2}(j-n_1-n_2 - [\tau_1' - (\tau_4' + \tau_5')])} \right\} + \left\{ > \rightarrow < n_1 n_2 \rightarrow -n_1, -n_2 \right\} \quad (3.3)$$

> and < refer to $n_1 + n_2 > 0$. There are five signatures $\tau_1 \dots \tau_5$ referring respectively to $j, \ell_1, \ell_2, n_1, n_2$ ($\tau_i' = \frac{1-\tau_i}{2}$). The signature factors differ slightly from II, and this is important if odd signature Regge poles are considered. The minus sign has appeared in (3.3) simply because of the rewriting of the two helicity sums in (3.1) in terms of contour integrals. It disappears again once the residue of helicity poles in

$$a_{>}^{\vec{\tau}}(j, \vec{\ell}, \vec{n}, t, t_1, t_2) \text{ at } \ell_1 = n_1 = \alpha(t_1), \ell_2 = n_2 = \alpha(t_2)$$

is taken by pulling the n_1 and n_2 contours in (3.3) to the left in their respective planes.

A further minus sign is introduced if, as in II, we use subenergy discontinuity formulae to replace

$$-\frac{1}{16\pi^2} \left(\frac{t_1 - 4m^2}{t_1} \right)^{\frac{1}{2}} \left(\frac{t_2 - 4m^2}{t_2} \right)^{\frac{1}{2}} a_{>}^{\vec{\tau}} a_{>}^{\vec{\tau}4--} \quad (3.4)$$

by $a_{>}^{\vec{\tau}} a_{>}^{\vec{\tau}4--} / a^{\tau_2} a^{\tau_3}$ (a^{τ_1} being the Froissart-Gribov continuation of the four-point function) and replace $\int d\rho$ by a contour integral around the two-particle thresholds at $t_1 = 4m^2$ and $t_2 = 4m^2$.

The residue of the helicity poles at $n_1 = \alpha(t_1)$ and $n_2 = \alpha(t_2)$ now contains a pole at $j = \alpha(t_1) + \alpha(t_2) - 1$ coming from the pole at

$j = n_1 + n_2 - 1$ in $\Lambda(j, \vec{\ell}, \vec{n})$. The collision of this pole with the boundary of the phase-space integral $\int d\rho$ generates the two-Reggeon cut. Before writing down the discontinuity formula we note that an important sign change comes from the signature factors in (3.3). Since these are evaluated at $j = n_1 + n_2 - 1$ we can write their collective contributions as

$$S_{\alpha_1 \alpha_2}^{\tau_1' \tau_4' \tau_5'} = \frac{\sin \frac{\pi}{2} (j - \tau_1')}{\sin \frac{\pi}{2} (\alpha_1 - \tau_4') \sin \frac{\pi}{2} (\alpha_2 - \tau_5') \sin \frac{\pi}{2} [-1 - \tau_1' + (\tau_4' + \tau_5')]} \quad (3.5)$$

If we now take α_1 and α_2 to be the Pomeranchukon so that

$\tau_1' = \tau_4' = \tau_5' = 0$ and $\alpha_1 \sim \alpha_2 \sim j \sim 1$ we obtain

$$S_{\alpha_1 \alpha_2}^{\tau_1' \tau_4' \tau_5'} = \frac{\sin \frac{\pi}{2} j}{\sin \frac{\pi}{2} \alpha_1 \sin \frac{\pi}{2} \alpha_2} \sim -1 \quad (3.6)$$

Taking account of the sign changes in (3.4) and (3.6) [and the removal of the - sign from (3.1) in taking the residue of helicity poles] the two Reggeon cut discontinuity obtained from (3.3) is equation (2.21) of II, that is (note that $a(j, t)$ which appears in the following formulae is the Froissart-Gribov amplitude which satisfies the Carlson condition in $t > 4m^2$, and differs from the amplitude which appears in (2.3) by a phase--see (4.3).]

$$\text{disc } a(j, t) \Big|_{j=j_c} = \text{disc } \Big|_{j=j_c} \left[\frac{i \sin \frac{\pi}{2} j}{\pi 2^7} \int \frac{dt_1 dt_2 \lambda^{1/2}(t, t_1, t_2)}{t(j - \alpha_1 + \alpha_2 + 1) \sin \frac{\pi}{2} \alpha_1 \sin \frac{\pi}{2} \alpha_2} \right. \\ \left. \times N_{\alpha}^{\sim}(j, t) N_{\alpha}^4(j, t) \right] \quad (3.7)$$

where

$$\text{disc } a(j, t) \Big|_{j=j_c} = a(j+i\epsilon, t) - a(j-i\epsilon, t) \quad (3.8)$$

and $N_{\alpha}^{\sim}(j, t)$, when evaluated at $j = \alpha_1 + \alpha_2 - 1$, is the "fixed-pole residue" of the particle/Reggeon scattering amplitude. $N_{\alpha}^4(j, t)$ is the same amplitude evaluated below its four-particle cut in the t -plane.

The singularity of the right-hand side of (3.7) occurs partly from the generation of the branch-point in the integral and partly from the presence of the cut in $N_{\alpha}^{\sim}(j, t)$ [but not in $N_{\alpha}^4(j, t)$]. In II we showed how the full unitarity equations for the six and eight-particle amplitudes could be manipulated to give the result that the complete discontinuity can be expressed as the discontinuity generated in the integral of (3.7), provided that $N_{\alpha}^{\sim}(j, t) N_{\alpha}^4(j, t)$ is replaced by $N_{\alpha}^{\sim}(j^+, t) N_{\alpha}^4(j^-, t)$. \pm refer to $\pm i\epsilon$ prescriptions in the j -plane with respect to the two-Reggeon cut in $N_{\alpha}^{\sim}(j, t)$. The final discontinuity formula we gave was therefore

$$\text{disc } a(j, t) = \frac{-\sin \frac{\pi}{2} j}{2^6} \int_{t_1^-}^{t_1^+} dt_1 \int \frac{dt_2 \lambda^{1/2}(t, t_1, t_2)}{t \sin \frac{\pi}{2} \alpha_1 \sin \frac{\pi}{2} \alpha_2}$$

$$\times \delta(j - \alpha_1 - \alpha_2 + 1) N_{\underline{g}}(j^+, t) N_{\underline{g}}(j^-, t) \quad (3.9)$$

where t^+, t^- are two solutions of $\lambda(t, t_1, t_2) = 0$ satisfying $j - \alpha(t_1) - \alpha(t_2) + 1 = 0$. The δ function is the result of formally taking the discontinuity of the branch-point generated in (3.7) when the pole at $j = \alpha_1 + \alpha_2 - 1$ hits the boundary of the phase-space at $\lambda(t, t_1, t_2) = 0$. However, because of the two-dimensional phase-space involved the collision of the pole with the boundary of the integration region is a little more subtle than (3.9) suggests. At this stage therefore, the δ -function in (3.9) must be regarded as symbolic only and representing $\frac{1}{2\pi i}$ x a Cauchy contour integral around the pole at $j = \alpha_1 + \alpha_2 - 1$, in a sense which we have yet to determine.

IV. ANALYTIC CONTINUATION TO $t \gtrsim 0$

In this section we consider continuation of the discontinuity formula down to t positive but near zero. We do this by using a simple $t + i\epsilon$ prescription for continuing past all other singularities encountered on the way. On general grounds we would expect this to be the right prescription for obtaining the high-energy behavior in the cross channel. In the next section we show that this has to be the case since this is the continuation which moves all mass-dependent singularities from the physical sheet of the j -plane.

The analysis in II which leads to (3.7) and (3.9) is all carried out above the four-particle threshold in the t -channel. Therefore in an

equal mass theory with mass m the formula is initially derived for $t \geq 16 m^2$. An important part of the continuation to small t is the treatment of threshold factors in $N_{\underline{\alpha}}(j, t)$, which have to be removed to obtain an amplitude which is real analytic for small t . This was discussed in II. We extract the threshold at $\lambda = 0$ in $N_{\underline{\alpha}}(j, t)$ by writing

$$N_{\underline{\alpha}}(j, t) = C_{\underline{\alpha}}(j, t) \left(\frac{\lambda}{t} \right)^{\frac{j - \alpha_1 - \alpha_2}{2}} \quad (4.1)$$

Since $N_{\underline{\alpha}}(j, t)$ is analagous to the Froissart-Gribov projection of an unequal mass scattering amplitude ($m + m \rightarrow t_1 + t_2$) it will also have threshold behavior of the usual form at $t = 4m^2$. Therefore, for $t < 4m^2$ it is $e^{i\frac{\pi}{2}j} C_{\underline{\alpha}}(j, t)$ which is real analytic and so satisfies*

$$\left[e^{i\frac{\pi}{2}j} C_{\underline{\alpha}}(j^+, t) \right]^* = \left[e^{i\frac{\pi}{2}j} C_{\underline{\alpha}}(j^-, t) \right] \quad (4.2)$$

[The $e^{i\frac{\pi}{2}j}$ factor in this equation is unfortunately replaced by $e^{i\pi j}$ in II, although this does not affect the final sign.]

The simplest way to deal with this last threshold behavior is to redefine $a(j, t)$ and $N_{\underline{\alpha}}(j, t)$ in (3.7) by multiplying by $e^{i\pi j}$ and $e^{i\frac{\pi}{2}j}$ respectively. If we similarly redefine $C_{\underline{\alpha}}(j, t)$ in (4.1), then we can rewrite (3.9) entirely in terms of amplitudes which are real analytic in $t < 4m^2$

$$\text{disc } a(j, t) = \frac{-\sin \frac{\pi}{2}j}{2^6} \int_{t_1^-}^{t_1^+} dt_1 \int dt_2 \frac{\delta(j - \alpha_1 - \alpha_2 + 1)}{\lambda^{1/2}(t, t_1, t_2)}$$

$$\times \left[\frac{C(j^+, t) C(j^-, t)}{\sin \frac{\pi}{2} \alpha_1 \sin \frac{\pi}{2} \alpha_2} \right] \quad (4.3)$$

where [] will be real and positive in $t < 4m^2$. $a(j, t)$ is now the amplitude which appears in (2.3).

To be specific about the definition of the δ -function in (4.3) we have to reconsider the generation of the branch-point in (3.7). We shall base our analysis on that of Simonov.⁶ For $t > 16m^2$ the projection of the integration region for (3.7) in the (t_1, t_2) plane is shown in Fig. 3. It is important to note that the boundaries of the integration region at $t_1 = 4m^2$, $t_2 = 4m^2$ are not fixed, but rather if we consider the projection of the integration region in the t_1 -plane (for fixed t_2) we see the integration contour shown in Fig. 4. This will be particularly important in the next section.

Consider the projection of the integration region in the plane of the variable $z = \alpha(t_1) + \alpha(t_2) - 1$. This is shown in Fig. 5. Since $\alpha(t)$ will be singular at $t = 4m^2$, the parts of integration contour which are on separate sheets of the t_1 and t_2 thresholds are separated in this plane. We denote the part of the contour with a $+i\epsilon$ prescription with respect to both thresholds by z_{++} , that with a $-i\epsilon$ prescription for t_1 only by z_{-+} etc. z_{++} and z_{-+} are shown in Fig. 5. We have drawn the relative positions of $z = 2\alpha\left(\frac{t}{4}\right) - 1$ and $z = \alpha\left[(\sqrt{t}-m)^2\right] + \alpha(4m^2) - 1$ differently from Simonov.⁶ It can easily be checked that our configuration is qualitatively correct if $\alpha(t)$ has a fractional power branch point at

$t = 4m^2$, as would be expected. Because of the symmetry of the integration region for z_{++} under $t_1 \leftrightarrow t_2$, the region for z_{++} shown in Fig. 5 is in fact covered twice, with the boundary between $2\alpha(\frac{t}{4}) - 1$ and $2\alpha(4m^2) - 1$ providing the link.

The pole at $j = \alpha(t_1) + \alpha(t_2) - 1$ appears as a single point at $z = j$. A singularity of the integral arises whenever the pole collides with one of the singular points of the boundary of the integration region. In this section we consider only the two-Reggeon branch-point which occurs when the pole collides with the singular point $z = 2\alpha(\frac{t}{4}) - 1$. [Note that this is not a singular point for z_{-+} , although $z = 2\alpha^*(\frac{t}{4}) - 1$ will be for z_{--} .] We, therefore, concentrate on the neighborhood of $z = 2\alpha(\frac{t}{4}) - 1$ in Fig. 5. We can add a third dimension to represent the two-dimensional nature of the integration for example, $\text{Re} [\alpha(t_1) - \alpha(t_2)]$. The resulting three-dimensional picture is shown in Fig. 6.

As we continue to $t < 16m^2$ (using a $+i\epsilon$ prescription) the point $z = 2\alpha(\frac{t}{4}) - 1$ moves down onto the real axis in an anti-clockwise direction around $t = 16m^2$. The shell of Fig. 6 flattens out and we obtain the picture shown in Fig. 7. The vital point is that for $j > 2\alpha(\frac{t}{4}) - 1$ the pole at $z = j$ lies above the integration region in the z -plane. That is it has a " $+i\epsilon$ " prescription relative to the integration region.

The integration contour has moved from a region $\lambda(t, t_1, t_2) > 0$ to a region in which $\lambda(t, t_1, t_2) < 0$ during the course of this continuation. Because of our $+i\epsilon$ prescription the contour has moved through the upper half λ -plane and so

$$\frac{1}{\lambda^{1/2}(t, t_1, t_2)} \rightarrow \frac{1}{i[-\lambda(t, t_1, t_2)]^{1/2}} = \frac{-i}{[-\lambda(t, t_1, t_2)]^{1/2}} \quad (4.4)$$

Since both the t_1 and t_2 integrations are reversed in direction by this continuation there is no net change of sign of the integration measure.

We can now evaluate a certain discontinuity in a simple way and this will be sufficient to check that we have the right sign for the Mandelstam graphs which we discuss in Sec. VII. Suppose that in the j -plane we continue down to $j = 2\alpha(\frac{t}{4}) - 1$ and continue around the branch point in an anti-clockwise direction. The pole at $z = j$ moves around the integration contour in the z -plane, as shown in Fig. 8. The resulting discontinuity in the integral around the pole at $z = j$ in the direction shown in Fig. 9. This together with a minus sign coming from the fact that the integral in (3.7) contains $(j-z)^{-1} = -(z-j)^{-1}$ tells us that the contour integral around the pole implied by (3.9) has to be interpreted as

$$- 2\pi i \delta(j - \alpha_1 - \alpha_2 + 1) \quad (4.5)$$

where the δ -function has the usual meaning

$$\int dt_2 \delta[j - \alpha(t_1) - \alpha(t_2) + 1] f(j, t_1, t_2) = \frac{1}{|\alpha'(t_2)|} [f(j, t_1, t_2)]_{j=\alpha_1 + \alpha_2 - 1} \quad (4.6)$$

Using (4.4) and (4.5) we therefore have that the discontinuity we have evaluated (\widetilde{disc}) is given by

$$\begin{aligned}
 \text{disc } \alpha(j, t) = & - \frac{i \sin \frac{\pi}{2} j}{2^6} \int_{t_1^-}^{t_1^+} dt_1 \int dt_2 \frac{\delta[j - \alpha(t_1) - \alpha(t_2) + 1]}{[-\lambda(t, t_1, t_2)^{1/2}]} \\
 & \times \left[\frac{C_{\alpha}(j^+, t) C_{\alpha}(j^-, t)}{\sin \frac{\pi}{2} \alpha(t_1) \sin \frac{\pi}{2} \alpha(t_2)} \right] \quad (4.7)
 \end{aligned}$$

This discontinuity is that obtained by drawing a branch cut to the right in the j -plane, rather than the left. $C_{\alpha}(j^+, t)$ will not be simply related to $C_{\alpha}(j^-, t)$ in general, and we cannot use the real analyticity property of $C_{\alpha}(j, t)$ to conclude that [] in (4.7) is real and positive. Also if we try to evaluate the discontinuity obtained by drawing the branch-cut to the left we encounter the complication that the integration region of Fig. 4.5 will be distorted to complex t_1 and t_2 by the pole at $j = \alpha(t_1) + \alpha(t_2) - 1$, if we continue around the branch-point in a clockwise direction. This problem can only be avoided by performing the further analytic continuation to negative t which we discuss in Sec. VI.

However, suppose we assume that $C_{\alpha}(j, t)$ has no branch-point at $j = 2\alpha(\frac{t}{4}) - 1$, as would be the case for the Mandelstam graphs. $C_{\alpha}(j, t)$ will then be real and the branch-point given by (4.7) will simply be logarithmic. The discontinuity evaluated either with the branch-cut drawn to the right or the left will be a simple imaginary constant and the only question remaining will be the sign. In fact since all factors in (4.7) apart from the overall minus sign, are now real and positive it follows that the discontinuity we have evaluated is negative. The discontinuity required for (2.3) is obtained by rotating the branch-cut through 180°

in the lower half j -plane as shown in Fig. 10. It follows then that

$$\frac{\text{disc } a(j, t)}{i} = \frac{1}{i} [a_1(j, t) - a_2(j, t)] = \frac{1}{i} [a(j-i\epsilon, t) - a(j+i\epsilon, t)] \quad (4.8)$$

$$< 0 \quad (4.9)$$

and so from (2.3) and (2.5) the cut will contribute negatively to the total cross section. This result is for the moment dependent on the neglect of the branch point in $C_g(j, t)$, but it is already sufficient to show that we will obtain the correct sign for the Mandelstam graphs and so confirms the correctness of our j -plane analytic continuation of multiparticle unitarity.

V. THE MASS-DEPENDENT SINGULARITIES

Further singularities besides the two-Reggeon cut will be generated in (3.7) as follows. A branch point at

$$j = \alpha[(\sqrt{t} - 2m)^2] + \alpha(4m^2) - 1 \quad (5.1)$$

will be generated when the integration contour is trapped by the pole at $j = \alpha(t_1) + \alpha(t_2) - 1$ together with the singularities of the integrand at $\lambda(t, t_1, t_2) = 0$ and t_1 or $t_2 = 4m^2$. Also a branch point will be generated at

$$j = 2\alpha(4m^2) - 1 \quad (5.2)$$

when the contour is trapped by the pole at $j = \alpha(t_1) + \alpha(t_2) - 1$ and the thresholds at both $t_1 = 4m^2$ and $t_2 = 4m^2$.

In terms of the z -plane projection of the integration contour shown

in Fig. 4.3 the branch points (5.1) and (5.2) arise when the pole at $z = j$ collides with the singular points of the boundary at $z = \alpha[(\sqrt{t}-2m)^2] + \alpha(4m^2) - 1$ and $z = 2\alpha(4m^2) - 1$ respectively. However, as we discussed in the last section, the boundaries of the integration region at $t_1, t_2 = 4m^2$ are not fixed and if the contour is extended below these points in the t_1 and t_2 -planes then the z_{++} integration region in Fig. 5 will be distorted as shown by the dotted line. This shows that the singularities (5.1) and (5.2) will only be generated if a path in the j -plane is taken so that the pole at $z=j$ moves along the path (i) shown in Fig. 5. In this case the boundary of the integration region can be trapped by the pole and the thresholds at t_1 and $t_2 = 4m^2$. However, if path (ii) is taken in the j -plane then the pole at $z=j$ and the thresholds will be on the same side of the contour and no trapping of the contour can occur.

Since paths (i) and (ii) involve different routes around the two-Reggeon cut it is clear that the mass-dependent singularities occur only on one sheet of the two-Reggeon cut. These singularities appear to the right of the two-Reggeon cut in the j -plane, for $t < 16m^2$. Therefore, they must be absent from the "physical sheet" of the two-Reggeon cut if the Froissart bound is not to be violated at $t = 0$.

If we draw the cut attached to the two-Reggeon branch point to the left in the j -plane, as in Fig. 11, then it follows from the above analysis that the singularities (5.1) and (5.2) can only be reached by "burrowing down" through the cut as indicated by the arrow. It should

then be clear that these singularities will indeed be on the unphysical sheet of the two-Reggeon cut for $t < 16 m^2$ if we use the $+i\epsilon$ prescription of the last section. In this case the branch point at $j = 2\alpha\left(\frac{t}{4}\right) - 1$ simply moves around $t = 16 m^2$ in an anti-clockwise direction leaving the sheets on which (5.1) and (5.2) are singular hidden.

In Ref. 7 we discussed the three-particle unitarity integral in detail and showed that the Reggeon-particle cut at $j = \alpha[(\sqrt{t} - m)^2] - 1$ is generated in that integral. The Reggeon-particle cut is a mass-dependent singularity which also moves onto the unphysical sheet of the two-Reggeon cut for small t . In II we showed that this happens by considering the generation of the Reggeon particle cut in the two-Reggeon cut discontinuity.

In fact there are other singularities at $j = \alpha(4m^2) - 1$ and $j = \alpha(0) - 1$ which are generated in the three-particle integral in the analogous way to the generation of (5.1) and (5.2) in the four-particle integral. The simplest way to show that these singularities also move onto the unphysical sheet of the two-Reggeon cut is to include the three-particle unitarity relation in the four-particle relation as discussed by Simonov.⁶ The full amplitude can then be reconstructed from a dispersion relation. We do not intend to discuss the details here and so we simply state Simonov's conclusion.

For $t > 16 m^2$ the two-Reggeon cut can shield these singularities as we have shown in Fig. 11. Using a $+i\epsilon$ prescription in the t -plane

the same sheet of the two-Reggeon cut is shown in Figs. 12 and 13 for $9 m^2 < t < 16 m^2$ and $t < 4m^2$ respectively. With the cut drawn as shown none of the other branch points are singular on the physical sheet.

VI. ANALYTIC CONTINUATION TO $t < 0$

Since $\lambda(t, t_1, t_2) \underset{t \rightarrow 0, t_1=t_2}{\sim} t^{1/2}$ it appears, at first sight, that (4.7) and also (3.7) may be singular at $t=0$. A simple way to see that this is not the case is to consider directly the integral

$$I(j, t) = \int_{\lambda < 0} dt_1 dt_2 \frac{1}{[-\lambda(t, t_1, t_2)]^{1/2} [j - \alpha(t_1) - \alpha(t_2) + 1 + i\epsilon]} \quad (6.1)$$

and rewrite this in terms of the variables

$$x = \frac{t_1 + t_2}{2} \quad y = \frac{t_1 - t_2}{2} \quad (6.2)$$

We assume that the trajectory is approximately linear at $t=0$.

[If we were to take $\alpha_p(0) < 1$ then we would expect the trajectory to be analytic at $t=0$ and this would be sufficient for the following argument. For $\alpha_p(0) = 1$ we are assuming that weak coupling takes place so that the trajectory function is only mildly affected by multi-Pomeranchukon cuts.] (6.1) becomes

$$I(j, t) = \int_{-\infty}^{\infty} dy \int_{\frac{t^2+y^2}{4t}}^{\infty} dx \frac{1}{(-t^2 + 4xt - y^2)^{1/2} (j - 2\alpha'x - 1 + i\epsilon)} \quad (6.3)$$

Changing variables, yet again, to

$$y' = y/t^{1/2} \quad x' = x - \frac{(t+y'^2)}{4} \quad (6.4)$$

$$I(j,t) = \int_{-\infty}^{\infty} dy' \int_0^{\infty} dx' \frac{1}{2[x']^{1/2}} \frac{1}{j - 2\alpha' [x' + \frac{t+y'^2}{4}] - 1 + i\epsilon} \quad (6.5)$$

which is clearly not singular at $t=0$, although (6.1) appears to be. We can now use Cauchy's theorem to perform two successive transformations on (6.5). First we rotate the x' -contour through 180° in the lower half x' -plane so that

$$\int_0^{\infty} dx' [x']^{-1/2} \rightarrow -i \int_{-\infty}^0 [-x']^{-1/2} dx' \quad (6.6)$$

Then we rotate the y' -contour through 90° so that

$$\int_{-\infty}^{\infty} dy' \rightarrow \int_{+i\infty}^{-i\infty} dy' = -i \int_{-\infty}^{\infty} dy'' \quad (6.7)$$

where $y' = i y''$. So now (6.5) becomes

$$I(j,t) = - \int_{-\infty}^{\infty} dy'' \int_{-\infty}^{\infty} dx' \frac{1}{2[-x']^{1/2}} \frac{1}{[j - 2\alpha' (x' + \frac{t-y''^2}{4}) - 1]} \quad (6.8)$$

The integration region and the pole in the integrand are shown in the (x', y'') plane in Fig. 14 for $j > \alpha' \frac{t}{4} + 1$ and it is obvious that the

discontinuity given by the collision of the pole and the boundary of the integration at $x' = 0$ is

$$I(j+i\epsilon, t) - I(j-i\epsilon, t) = +\pi i \int dy'' \int \frac{dx'}{[-x']^{1/2}} \delta \left[j - 2\alpha'(x' + \frac{t-y''^2}{4}) - 1 \right] \quad (6.9)$$

(6.1) corresponds directly to (3.7) (evaluated for $t \geq 0$) if we insert (4.1) and (4.4) and ignore both the branch-point in $C_{\mathcal{L}}(j, t)$ and all other irrelevant factors. Since the integration in (6.9) is over imaginary $y = \frac{t_1 - t_2}{2t^{1/2}}$, it will be over complex values of t_1 and t_2 for t positive. This is why we did not use (6.9) for positive t in Sec.IV. However, we can use (6.1) - (6.9) to continue (3.7) to negative t and take the discontinuity we want. Imaginary y' corresponds to real t_1 and t_2 for negative t and so (6.9) gives directly that for negative t

$$\begin{aligned} \text{disc } a(j, t) = & + \frac{i \sin \frac{\pi}{2} j}{2^6} \int_{t_1^-}^{t_1^+} dt_1 \int dt_2 \frac{\delta(j - \alpha_1 - \alpha_2 + 1)}{[-\lambda(t, t_1, t_2)]^{1/2}} \\ & \times \left[\frac{C_{\mathcal{L}}(j^+, t) C_{\mathcal{L}}(j^-, t)}{\sin \frac{\pi}{2} \alpha(t_1) \sin \frac{\pi}{2} \alpha(t_1)} \right] \end{aligned} \quad (6.10)$$

Since all factors in (6.10) apart from the i are now real and positive, it follows from (2.3) that the two-Pomeranchukon cut contributes negatively to the total cross section.

VII. THE MANDELSTAM GRAPHS

In this section we shall show that previous studies⁸⁻¹⁰ of the

Mandelstam graphs in weak-coupling. ϕ^3 perturbation theory can be used to check our analytic continuation.

The Mandelstam graphs are the set of Feynman graphs shown in Fig. 15. This set of graphs satisfies t-channel unitarity to a limited extent. Firstly, the lowest intermediate state in the t-channel is the four-particle state and the discontinuity is of the form shown in Fig. 1. The six-particle amplitude appearing on the right-hand side of Fig. 1 is shown in Fig. 16. This set of graphs also satisfies two-particle unitarity in both the t_1 and t_2 subchannels as illustrated in Fig. 17. The relevant four-point function now being the set of ladder graphs. It follows then that the Mandelstam graphs satisfy all of the t-channel unitarity equations necessary to obtain (3.7) (apart from those needed to study iterations of the two-Reggeon cut.) Therefore, our analysis must apply directly to the two-Reggeon cut asymptotic behavior of the Mandelstam graphs. In particular, then, our analytic continuation must give the correct sign.

These graphs can, of course, only be analysed in detail in the weak coupling limit, when the trajectory $\alpha(t) = -1 + 0(g^2)$, so that the trajectory of the two-Reggeon cut is $\alpha_c(t) = -3 + 0(g^2)$. Also, as Halliday and Sachrajda emphasize,¹⁰ the known minus sign for the two-Reggeon cut depends crucially on adding both untwisted and twisted ladder graphs so that the ladder graph Reggeons have definite (even) signature. In this case $\tau' = \tau'_1 = \tau'_2 = 0$, $\alpha_1 \sim \alpha_2 \sim -1$, $j \sim -3$ and we have from (3.5) that

$$S_{\alpha_1 \alpha_2}^{\tau'_1 \tau'_4 \tau'_5} \sim \frac{\sin(-\frac{3\pi}{2})}{(\sin-\frac{\pi}{2})^2 \sin(-\frac{\pi}{2})} = -1 \quad (7.1)$$

Therefore, $S_{\alpha_1 \alpha_2}^{\tau'_1 \tau'_4 \tau'_5}$ has the same sign as for the two-Pomeranchukon cut and since all other factors are the same our analysis will give a negative sign for the Mandelstam graphs.

Note that if we took $\tau_4 = \tau_5 = +1$ we would obtain

$$S_{\alpha_1 \alpha_2}^{\tau'_1 \tau'_4 \tau'_5} \sim \frac{+1}{\sin \frac{\pi}{2}(\alpha_1 - 1) \sin \frac{\pi}{2}(\alpha_2 - 1)} \gg 1 \quad (7.2)$$

so that for odd-signature Reggeons we obtain a positive sign. For unsigned ladders in the Mandelstam graphs, we effectively have degenerate Regge trajectories of both signatures. Since (7.2) is much larger than (7.1) the positive sign contribution will dominate over the negative sign contribution and we will again obtain the correct positive sign for the unsigned Mandelstam graphs.

VIII. DISCUSSION--MULTI-POMERANCHUKON CUTS

It is clear from our comparison with the Mandelstam graphs in the last section that it is the treatment of signature that is the vital factor in giving the negative sign for the two Pommeranchukon cut. The various minus signs and factors of i which arise in (3.4), (4.4) and (4.5) from phase-space factors and analytic continuation problems all cancel and the controlling factor is the "signature factor" $S_{\alpha_1 \alpha_2}^{\tau'_1 \tau'_4 \tau'_5}$ defined in (3.5). This result is also in agreement with Gribov's treatment of hybrid Feynman diagrams leading to the Reggeon calculus.¹² In Gribov's work it is the "signature factor" which gives the negative sign for the two Pommeranchukon cut.

In fact we can really trace the sign to the last factor in the denominator of (3.5), that is

$$\begin{aligned} \sin \frac{\pi}{2} [-1 - \tau'_1 + (\tau'_4 + \tau'_5)] &\equiv \sin \frac{\pi}{2} [j - n_1 - n_2 - \tau'_1 + (\tau'_4 + \tau'_5)] \\ &= \sin \frac{\pi}{2} (j - n_1 - n_2) \text{ for } \tau'_1 = \tau'_4 = \tau'_5 = 0 \end{aligned} \quad (8.1)$$

This factor arises from our Sommerfeld-Watson transformation of the helicity sums in the four-particle unitarity relation and $j - n_1 - n_2 = -1$ because of the generation of the two Reggeon cut by the nonsense wrong-signature fixed-pole at $j = n_1 + n_2 - 1$. It is clear from the work of Gribov, Pommeranchukon and Ter Martirosyan¹ that two nonsense fixed-poles are involved in generating the three-Reggeon cut in the six-particle unitarity

integral as illustrated in Fig. 18. First two Regge poles at $\ell_2 = n_2 = \alpha(t_2)$, $\ell_3 = n_3 = \alpha(t_3)$ and a nonsense fixed-pole at $\ell_1 = n_1 = n_2 + n_3 - 1$ give a pole in the n_1 -plane at $n_1 = \alpha(t_2) + \alpha(t_3) - 1$. This combines with a Regge pole at $n_4 = \ell_4 = \alpha(t_4)$ and a nonsense fixed pole at $j = n_1 + n_4 - 1$ to give a pole at $j = \alpha(t_2) + \alpha(t_3) + \alpha(t_4) - 1$ and this finally leads to the three-Reggeon cut. It seems reasonable to assume that, as for the two Reggeon cut, all minus signs coming from phase-space factors cancel so that the overall sign of the three-Reggeon cut will be governed by the signature factors. Since there will now be two factors of the form of (8.1) we can expect the sign of the three-Pomeranchukon cut to come out positive.

In general the generation of the N-Reggeon cut in the 2N particle unitarity integral involves (N-1) nonsense fixed-poles and so we expect that the N-Pomeranchukon cut will contribute to the total cross section with a factor $(-1)^{N-1}$. This is, of course, in agreement with Gribov's treatment of hybrid Feynman diagrams¹² but it is interesting to see that we can expect the result to emerge in a general way from t-channel unitarity.

REFERENCES

- ¹V. N. Gribov, I. Ya Pomeranchuk and K. A. Ter-Martirosyan, Phys. Rev. 139B, 184 (1965).
- ²A. R. White, Nucl. Phys. B50, 130 (1972) referred to as II in this paper.
- ³H. D. I. Abarbanel, Phys. Rev. D6, 2788 (1972).
- ⁴G. F. Chew, Phys. Rev. D7, 934 (1973).
- ⁵A. R. White, Nucl. Phys. B39, 461 (1972).
- ⁶Yu A Simonov, Zh ETF 48, 242 (1965), (Sov. Phys), JETP 21, 160 (1965).
- ⁷A. R. White, Nucl. Phys. B50, 93 (1972).
- ⁸G. M. Cicuta and R. L. Sugar, Phys. Rev. D3, 970(1971).
- ⁹B. Hasslacher and D. K. Sinclair, Phys. Rev. D3, 1770 (1971).
- ¹⁰I. G. Halliday and C. T. Sachwajda, Phys. Rev. D8, 3598 (1973).
- ¹¹R. J. Eden, P. V. Landshoff, D. I. Olive and J. C. Polkinghorne, the Analytic S-Matrix (Cambridge University Press, 1966).
- ¹²V. N. Gribov, Zh. Eksp. Teor. Fiz. 53, 654, Soviet Physics JETP 26, 414 (1968).

FIGURE CAPTIONS

- Fig. 1 Four-particle unitarity.
- Fig. 2 Partial-wave coupling scheme.
- Fig. 3. Integration region for the four-particle unitarity integral.
- Fig. 4 Projection in the t_1 -plane.
- Fig. 5 Projection in the z -plane.
- Fig. 6 The contour in three dimensions.
- Fig. 7 The contour in $t < 16 m^2$.
- Fig. 8 Movement of the pole at $z=j$.
- Fig. 9 The Cauchy integration around the pole.
- Fig. 10 Rotation of the branch cut in the j -plane.
- Fig. 11 The j -plane for $t > 16 m^2$.
- Fig. 12 The j -plane for $4 m^2 < t < 16 m^2$.
- Fig. 13 The j -plane for $t < 4 m^2$.
- Fig. 14 The integration region in the (x', y'') plane.
- Fig. 15 The Mandelstam graphs.
- Fig. 16 The $2 \rightarrow 4$ amplitude.
- Fig. 17 Sub-channel unitarity.
- Fig. 18 Generation of the three-Reggeon cut.

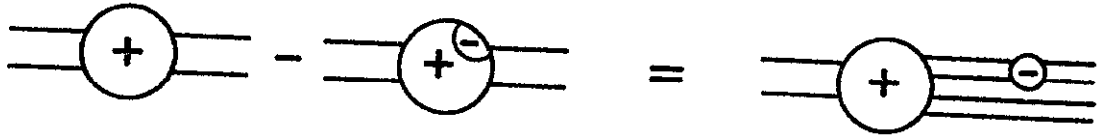


FIG.17

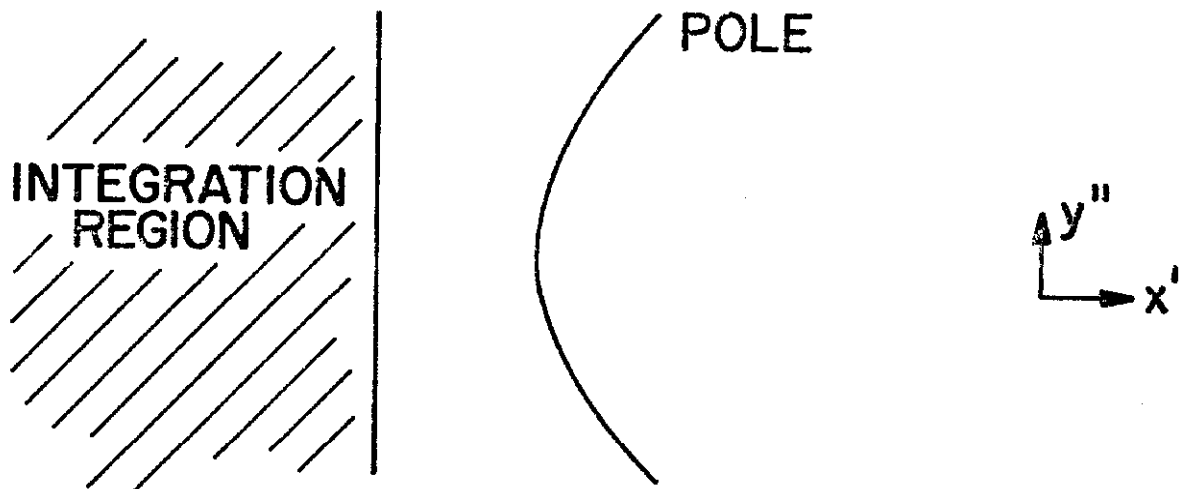


FIG. 14

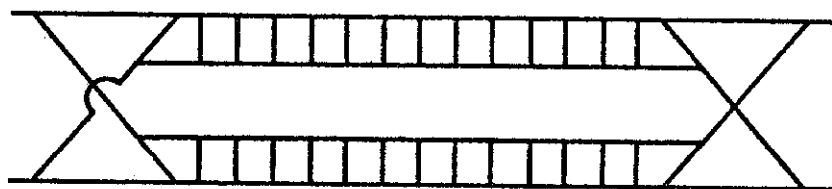


FIG. 15

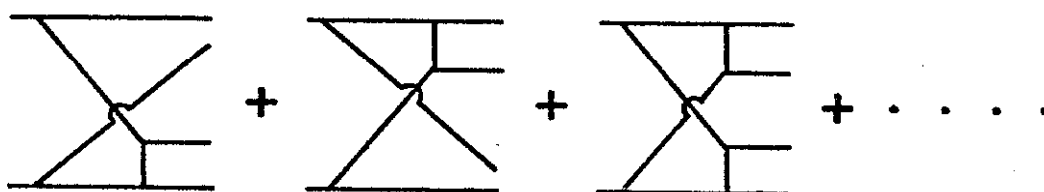


FIG. 16

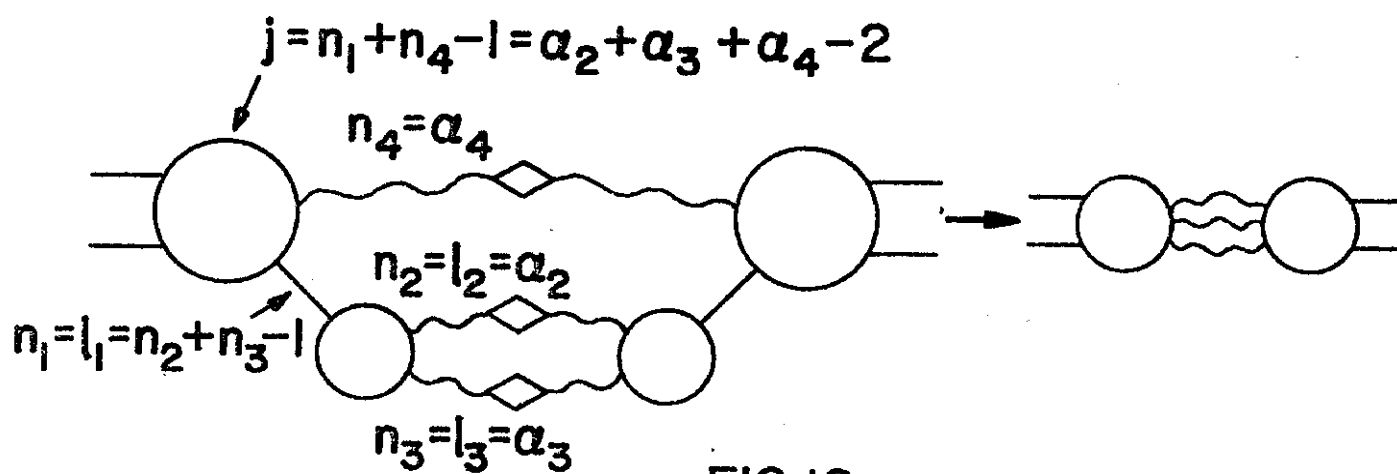


FIG. 18

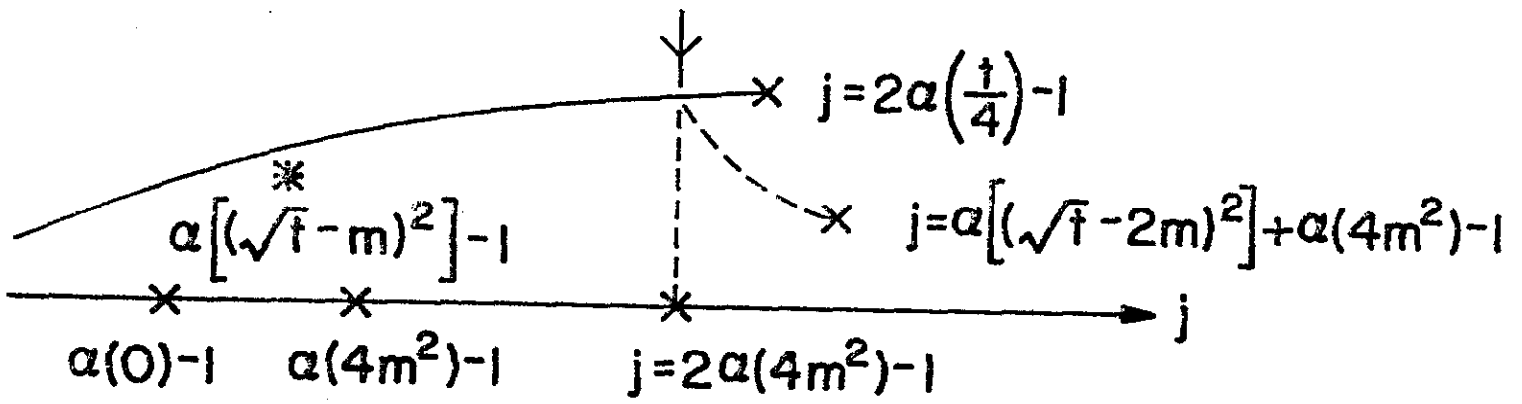


FIG. 11

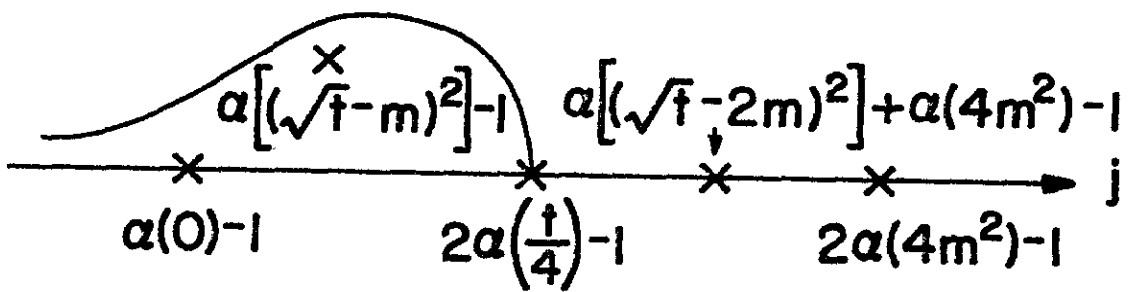


FIG. 12

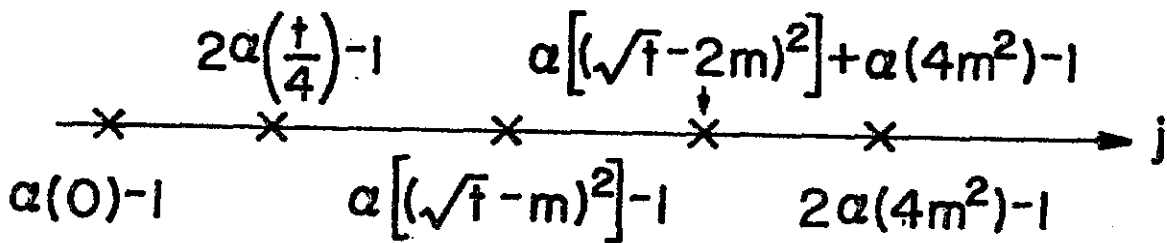


FIG. 13

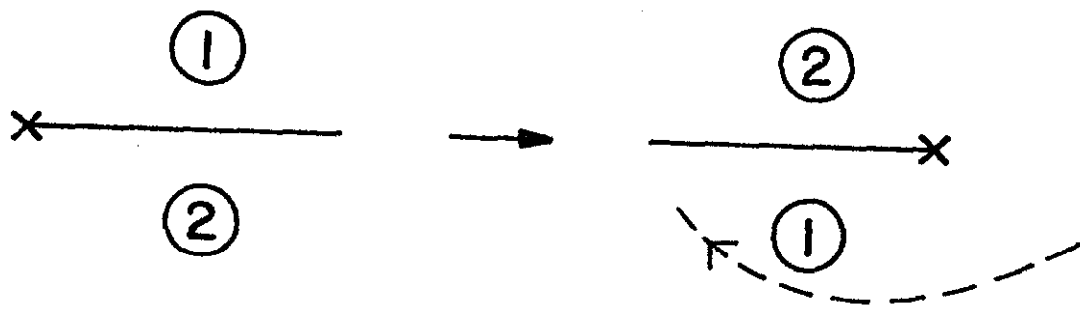


FIG. 10

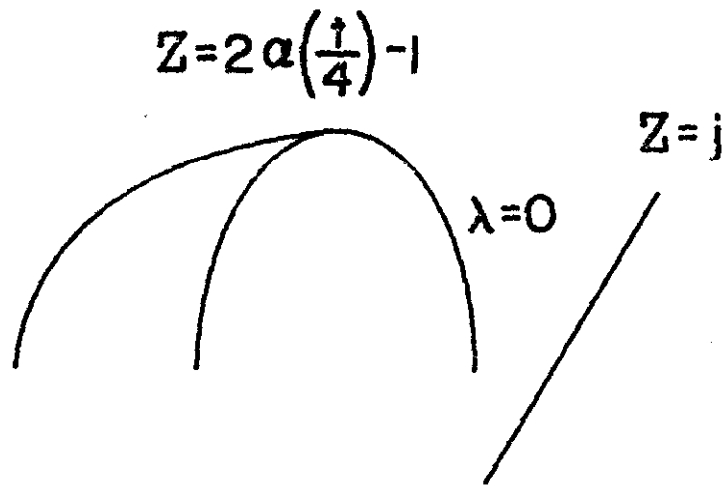


FIG. 6

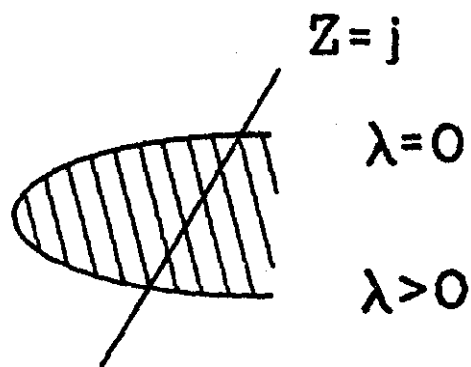


FIG. 7



FIG. 8



FIG. 9

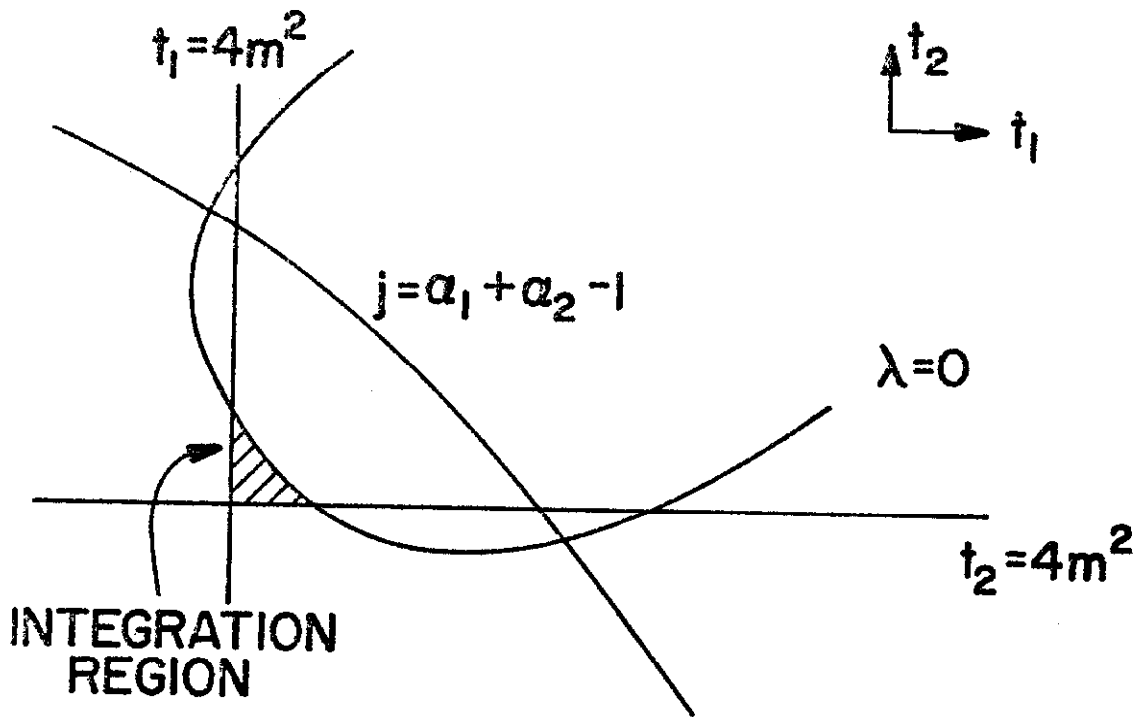


FIG. 3



FIG. 4

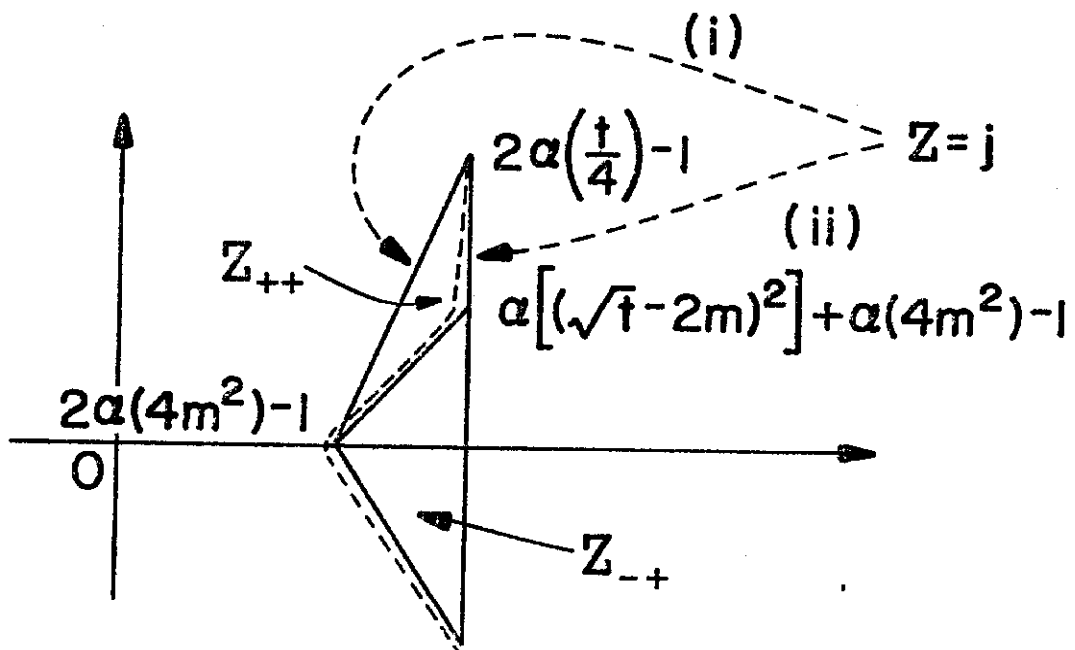


FIG. 5

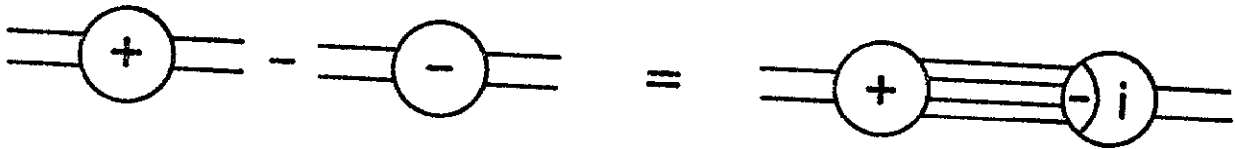


FIG. 1

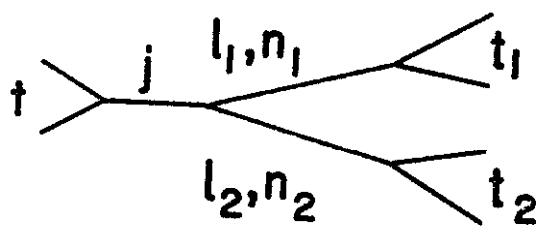


FIG. 2